 doi:10.20944/preprints201911.0048.v1

Article

Crystallographic and Seismic Anisotropies of Calcite at Different Depths: A Study Using Quantitative Texture Analysis by Neutron Diffraction

Michele Zucali [1,2], Daniel Chateigner [3] and Bachir Ouladdiaf [4]

[1] Università degli Studi di Milano, Italy; michele.zucali@unimi.it
[2] University of Houston, Texas - USA; mzucali@uh.edu
[3] University of CAEN - France; daniel.chateigner@ensicaen.fr
[4] ILL, Grenoble - France; oulad@ill.eu
* Correspondence: michele.zucali@unimi.it; Tel.: +1-346-383-9414

Abstract: Eight samples of limestones and marbles were studied by neutron diffraction to collect Quantitative Texture (i.e. Crystallographic Preferred Orientations or CPO) of calcite deforming at different depths in the crustal profile. We studied the different CPO patterns developed in shear zones at different depth and their influence on seismic a nisotropies. Samples were collected in the French and Italian Alps, Apennines and Paleozoic Sardinian basement. They are characterized by different mesoscopic fabrics, from isotropic to highly anisotropic (e.g. mylonite shear zone). Mylonite limestones occur as shear zone horizons within the Cenozoic Southern Domain in Alpine thrust-and-fold belts (Italy), the Briançonnais domain of the Western Alps (Italy-France border), the Sardinian Paleozoic back-thrusts or in the Austroalpine Upper units. The analyzed marbles were collected in the Carrara Marble, in the Austroalpine Units in the Central (Mortirolo) and Western Alps (Valpelline). The temperature and depth of development of the fabrics vary from shallow, < 100°C, to more than 800°C at depth of about 30 km. Quantitative Texture Analysis shows different types of patterns for calcite CPO, from random (Type A) to strongly textured (Type B); Type B may be further separated in orthorhombic and monoclinic, based on the angle defined with the mesoscopic fabrics, namely the shear p lane. Seismic anisotropies were calculated by homogenizing the single crystal elastic tensor, using the Orientation Distribution Function calculated by the Quantitative Texture Analysis. The resulting P- and S-waves anisotropies show a wide variability due to the textural types, depth within the crustal profile, and dip of the shear planes.

Keywords: calcite; seismic anisotropy; texture; CPO; thrust; shear zone; neutron diffraction; crust

1. Introduction

The quantification of the seismic response of rocks is a fundamental task in understanding Earth's structure, from the core to the surface [1]. The large-scale seismic experiments, now with high-resolution arrays, is the most used approach to image the Earth and to resolve the distribution of natural resources in-depth, e.g. water, ore minerals, and oil & gas [2,3]. However, the interpretation of seismic images strongly relies on the knowledge of the seismic response of the anisotropic aggregates of minerals composing the rocks as well on the main structural features [4]. In the last two decades, a great effort has been made to quantify the seismic response of natural aggregates, chiefly by using the 2Dimensional approach of the EBSD (Electron Back Scattered Diffraction) to reconstruct the Orientation Distribution

 doi:10.20944/preprints201911.0048.v1

Function (e.g. [5–7]). Carbonatic rocks mainly occur at the surface and at shallow levels, as sedimentary cover, but can be found with the crust, as marbles. At shallow levels, the tectonic deformation localizes, within the sedimentary cover, producing thrust-folds systems; weakness horizons often occur in carbonatic rocks [8]. Though less diffuse with the metamorphic basements, carbonatic rocks are known to be equally crucial at depth because the likely represent the main weak horizons, separating tectonometamorphic units [9,10]. For these reasons, the knowledge of the texture and seismic response of carbonatic rocks is important to interpret seismic profiles, at various depth within the crust. Several works have been dedicated to the study of calcite single crystal, limestones and calcitic marbles behaviors at different temperature and pressure [11–16]; a general scheme of the expected textural behavior has been developed, combining natural and numerical data (see [17] and references therein) but data are still needed. Moreover, virtually no work has been dedicated to combine the neutron diffraction textural data (Lattice Preferred Orientation) with the prediction of seismic velocities through the homogenization of the elastic tensor. This work starts filling this gap, with a compilation of natural data, analyzed by neutron diffraction; this proposed samples have been collected mainly in the Alpine system and provide a selection of carbonatic rocks showing various degree of planar fabrics, developed at different depth within the crust. Through this manuscript, the textural data (Orientation Distribution Function - ODF) will be used to calculate the homogenized elastic tensor. The resulting tensors are then used to calculate the seismic velocities reflecting the mineral composition of the rocks and their fabrics. The resulting velocities are finally used to predicted, in simple 2D model, the possible seismic images given by carbonatic rocks at various depth and with variably dipping fabrics, as is the common case in natural settings where carbonatic rocks are often found as shear horizons at various depth and varying dips.

2. Samples description and geological setting

Samples were collected in the French and Italian Alps, Apennines and Paleozoic basement (Figure 1). Different locations, shown in Figure 1, were chosen to sample carbonate rocks from different crustal levels, from shallow limestones to high-temperature marbles (Table 1). According to Figure 1, shallower samples were collected in the Southalpine domain, Sardinia and Helvetic-Deuphinoise (e.g. Triassic and Jurassic limestones). All samples preserve at macroscopic scale their primary features; intermediate depth samples were collected in the Briançonnais domain and in the Central Austroalpine domain, where Mesozoic sediments were involved in the Alpine tectonics at relatively shallow levels, but they still preserve their stratigraphic relations with the surrounding rocks, as well sedimentary features, such as strata or laminations. The last group of samples, collected in the Carrara metamorphic complex, and in the Western-Central Austroalpine domain, are metamorphic marbles. In this last group, no more sedimentary features are preserved. The samples location is reported in Figure 1, while Table 1 report basic geological information.

- The BAS sample, is an undeformed limestone, Jurassic in age from the Helvetic-Deuphinoise sedimentary cover, close to Grenoble (France).
- The SOD was collected in the Southalpine domain, it is Triassic in age and it is characterized by a well developed mylonite foliation, related to the thrust-tectonics during Alpine convergence.
- SA1 sample was collected in the Sardinia basement. It is part of the Ceroidi Limestone (Gonnesa Fm.), Cambrian cover involved in the Paleozoic tectonics. During this tectonic activity, a mylonitic foliation developed which is associated with low-grade metamorphic conditions.
- STE sample was collected in the Central Alps Upper Austroalpine sedimentary cover, strongly involved in the Alpine tectonics. It is characterized by a strongly developed mylonite fabric, associated with thick-thrust tectonics which involved slices of Austroalpine (previous Southalpine) continental crust and Paleozoic-Mesozoic cover.

Preprints (www.preprints.org) | NOT PEER-REVIEWED | Posted: 6 November 2019 doi:10.20944/preprints201911.0048.v1

- CC sample was collected in the Western Alps, in the sub-Briançonnais domain. It consists of Jurassic limestone strongly deformed during Alpine thrusting of the external part of the chain.
- P1 was collected in the well-known Carrara marble quarries. They consists of marbles of Alpine age produced during the Alpine-Apennines collision. It is commonly characterized by isotropic equigranular texture of recrystallized calcite.
- VP3 and MA1 represent lower crust marbles, produced during high-temperature Permian-Triassic extension of the Pangea. VP3 was collected in the Valpelline Series, Austroalpine of the Western Alps, while MA1 was collected in the Languard-Campo, Central Austroalpine Domain.

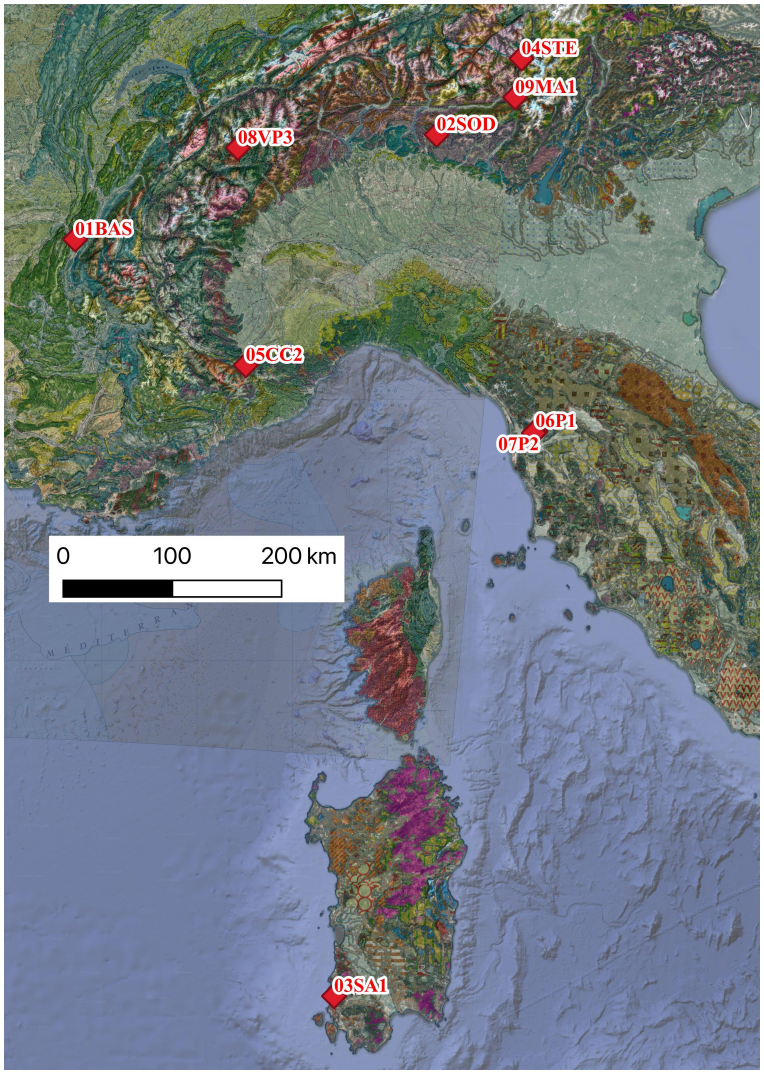

Figure 1. Location of studied samples. Geological maps after [18,19]

Preprints (www.preprints.org) | NOT PEER-REVIEWED | Posted: 6 November 2019 doi:10.20944/preprints201911.0048.v1

Table 1. Geological information about samples. Labels used in Figure 1 and in the text

Label	Domain	Crustal Position	mesoscopic anisotropy	Temperature
01BAS	Helvetic-Delphinoise	shallow	NO	very low
02SOD	Southalpine	shallow	YES	low
03SA1	Sardinia Basement	upper	YES	int
04STE	Upper Austrolpine	upper	YES	int
05CC2	Brianconnaise	upper	YES	int
06P1	Carrara Metamorphic Complex	lower	NO	int
08VP3	Austroalpine	lower	YES	high
09MA1	Austroalpine	lower	YES	high

3. Sample Reference System and Methods

The samples were cut in cubes of ≈ 1cm edge (Figure 2); the three axes of the cube correspond to the orthorhombic reference of the sample. In this orthorhombic Sample Reference System, the plane XY corresponds to the stratification or shear plane, while X direction is taken parallel to the flow direction or lineation, if it exists (Figure 2). The references in figure 2b is used in all the Pole Figures (Figures 3, 4, 5).

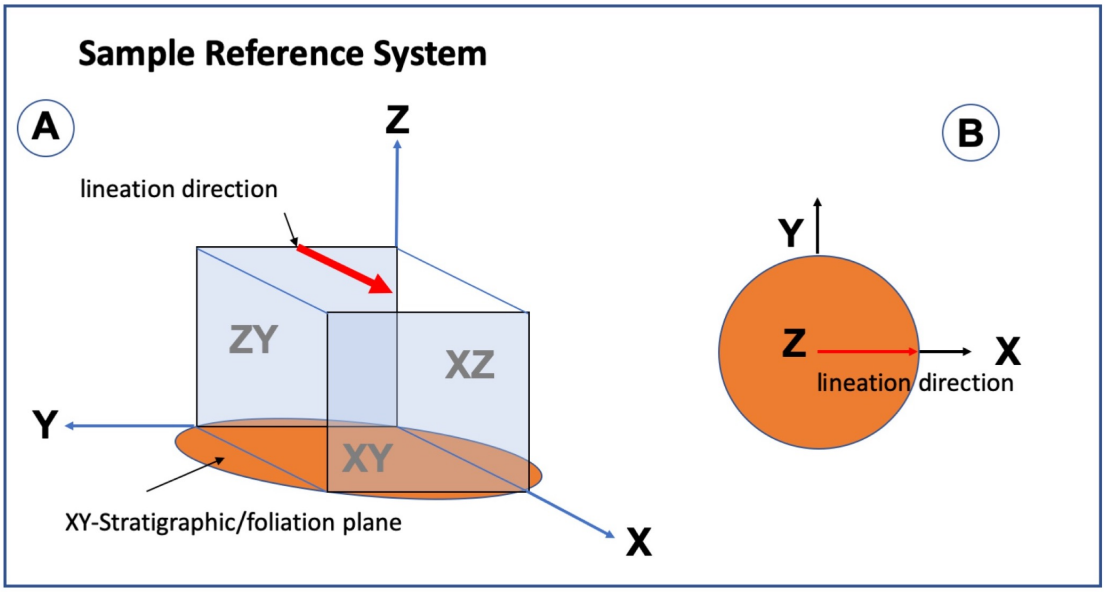

Figure 2. Sample Reference System and Pole figure representation. (**a**) Sample Reference System showing a simplified cubic sample with respect to the orthorhombic reference. X, Y and Z axes are shown (**b**) Pole figure reference representation with X, Y and Z axes.

In order to evaluate the **Crystallographic Preferred Orientation (CPO)** of the samples we used the non-disruptive method of the Quantitative Texture Analysis (QTA) by neutron diffraction, successfully applied on various types of rocks and synthetic materials: in monomineralic quartzites [20], marbles [17], limestones [21], dunite [22] or glaucophanite [23], in poly-phasic rocks, as amphibolite [24,25], quartz-feldspatic mylonitic orthogneisses and gabbros [26,27], subacqueous lavas [28] or sandstones [29]. This procedure uses the high penetration and high flux of neutrons available at the nuclear reactor at the Institute Laue-Langevin (Grenoble, France) allowing the measurement of samples with volumes of approximately 1 cm3 in one to few hours [30]. Here, we present the results from the D1B, D20 and D19 diffractometers (http://www.ill.eu). The raw data have been analyzed using the software package

Preprints (www.preprints.org) | NOT PEER-REVIEWED | Posted: 6 November 2019 doi:10.20944/preprints201911.0048.v1

MAUD (Materials Analysis Using Diffraction: [31]). Diffracted intensities are used to calculate the Orientation Distribution Function (ODF; [32]) from which the representative lattice planes are extracted and represented as Pole Figures (PF). PFs were represented showing the reference axes from the Sample Reference System (X, Y, Z in Fig. 2). The coverage of the three dimensional sample space has been acquired differently at the three beam lines, due to their technical specifications. The respective angular settings are reported in Table 2. The ODF was calculated using the E-WIMV approach [32]. The reliability of the refinement is shown by the refinement parameters reported in Table 3. Calcite lattice parameters used for the refinements are a = 4.9849 c = 17.0479. 2Theta off-set, sample position, and background parameters were also refined.

Table 2. ILL instrument, setup and DOI

SAMPLE	INSTRUMENT	year	omega	phi	chi	acq. time	http://doi.ill.fr/10.5291/ILL-DATA.
01BAS	D1B	2016	10	0-355	0-90	20	1-02-201
02SOD	D1B	2016	10	0-355	0-90	20	1-02-201
03SA1	D19	2014	10	0-355	0-90	10	5-11-397
04STE	D1B	2016	10	0-355	0-90	20	1-02-163
05CC2	D1B	2016	10	0-355	0-90	20	1-02-201
06P1	D1B	2014	10	0-355	0-90	20	1-02-163
08VP3	D20	2005	10	0-355	0-90	40	no DOI
09MA1	D20	2005	10	0-355	0-90	40	no DOI

Table 3. Quantitative Texture Refinement parameters

SAMPLE	Rb ref	Rexp ref	Rw ewimv	Rb ewimv	F2
01BAS	7.31	7.56	3.76	4.46	1.04
02SOD	24.6	5.93	2.9	4.0	1.10
03SA1	27.19	25.62	24.11	24.43	1.732
04STE	19.6	6.24	9.53	9.59	1.6
05CC	9.22	3.96	4.11	4.57	1.26
06P1	15.79	6.28	4.85	5.95	1.005
08VP3	31.01	4.05	10.44	11.02	2.17
09MA1	22.83	4.98	12.91	15.73	1.18

The **Seismic Properties** can be obtained using petrofabric data as extensively explained by [6]. Here we calculated the seismic properties by averaging the single crystal elastic tensor [33] by the ODF, as obtained by neutron texture analysis. In practice, the ODF calculated using the Maud procedure was used to homogenize the single crystal tensor in Maud. The resulting homogenized tensors were used in MTEX to compute and plot seismic properties [34]. Pole figures with the same reference system as those in texture analysis were used. Although various averaging procedures can be adopted [35], we used the arithmetic mean of the [36]. This approach to compute seismic velocities generally produces higher values when compared to natural samples. The reason why higher values are commonly obtained, it is that other important factors, intrinsic and extrinsic, controlling seismic velocities are not included in the calculation. Main factors controlling the seismic velocities in natural rocks are fluid pressure, cracks density and orientation, porosity, grain boundaries shape and preferred orientation [37–40].

A **thermodynamic approach** [25] was also used to calculate the seismic properties, at different pressure and temperature conditions, roughly corresponding to the estimate conditions of texture development of the studied samples. We used the PerpleX software package [41] to compute the seismic parameters as dependent on the thermodynamic function G (molar Gibbs free energy), which is minimized

Preprints (www.preprints.org) | NOT PEER-REVIEWED | Posted: 6 November 2019 doi:10.20944/preprints201911.0048.v1

to establish phases, amounts and compositions, stable as a function of pressure and temperature. The software requires chemical composition of the system as input. Software and data used for the calculation of phase relations and seismic velocities are freely available at http://www.perplex.ethz.ch. The graphical output was obtained using pyWerami source [42]. The calculated seismic properties can be seen as those of a polycrystal rock with no preferred orientations.

4. Results

4.1. Textures - CPO

Figure 3 also reports the calculated PFs for a single crystal of calcite, an aggregate of equigranular randomly-disposed crystals, and an aggregate of equigranular grains, by a statistical Fibre distribution.

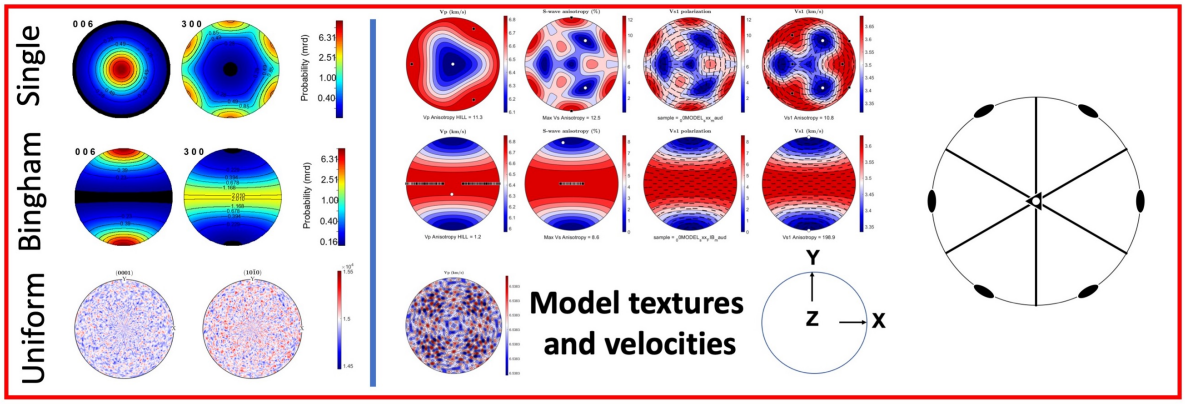

Figure 3. Pole Figures for model Textures (CPO) and Seismic Velocities for Single Crystal, Uniform and Bingham Textured samples

These references show the contributions to CPO expected by the crystallographic symmetry only or by textures: i) single crystal distribution is characterized by a strong c-axis maximum and a three-fold axes distribution in the plane normal to the c-axis; ii) oppositely, a random or uniform distribution of equigranular aggregate will reduce or obliterate the crystal symmetry anisotropy, producing a random statistical distribution, in any directions of the 3d space; iii) lastly, an imposed (e.g. tectonic stress) distribution, here represented as the Fibre Bingham distribution [43], will produce strong maxima that do not follow neither the crystal symmetry and nor a random distribution.

Figure 4 reports the pole figures representing the CPO measured for the studied samples. Bearing those end-members in mind, the PFs for the analyzed samples may be described. In figure 4 the same two lattice planes are represented (i.e (006) and (300)). Calcite texture are commonly expressed showing c and a axes distributions (e.g. (006) and (300) in our samples) since these axes better describe the deformation mechanisms active during plastic deformation at lattice scale. Table 3 reports comparison is made by the R factors and F2 factor, commonly used in texture analysis to asses the quality of refinement. In general, the samples show different texture distributions and intensities but they can be divided into 2 principal types: type A, random distribution (01BAS, 06P1); type B, c-axis fiber distribution (02SOD, 03SA1, 04STE, 05CC2, 08VP, 09MA). If the symmetry of the Pole Figures with the fabric elements is used, type B may be further divided into orthorhombic (02SOD, 05CC2, 09MA) and monoclinic symmetry (03SA1, 04STE, 05VP) types. By this features, the orthorhombic type is characterized by parallelism between the (006) poles and the Z direction, orthogonal to the shear or stratification plane; on the other hand, monoclinic type shows an angle between the (006) poles cluster and the Z direction. Symmetrically, the (300) poles, which generally

Preprints (www.preprints.org) | NOT PEER-REVIEWED | Posted: 6 November 2019 doi:10.20944/preprints201911.0048.v1

display a girdle distribution, may lay orthogonal to the Z direction (i.e. orthorhombic) or with an angle, generally 30 to 45 degrees. F2 values (Table 3) may be used as qualitative index to asses the randomness of the texture [44,45] even if its value is strongly controlled by microstructural heterogeneities such as grain size. As expected for poorly textured samples, 01BAS, 06P1 have F2 close to 1, even though 01BAS displays a minimum amount of preferred orientation. 02SOD, 04STE, 05CC2 and 09MA are characterized by well developed textures, though the F2 index is relatively low, being between 1.10 and 1.26. Highest F2 values are shown by 03SA1 and 09MA.

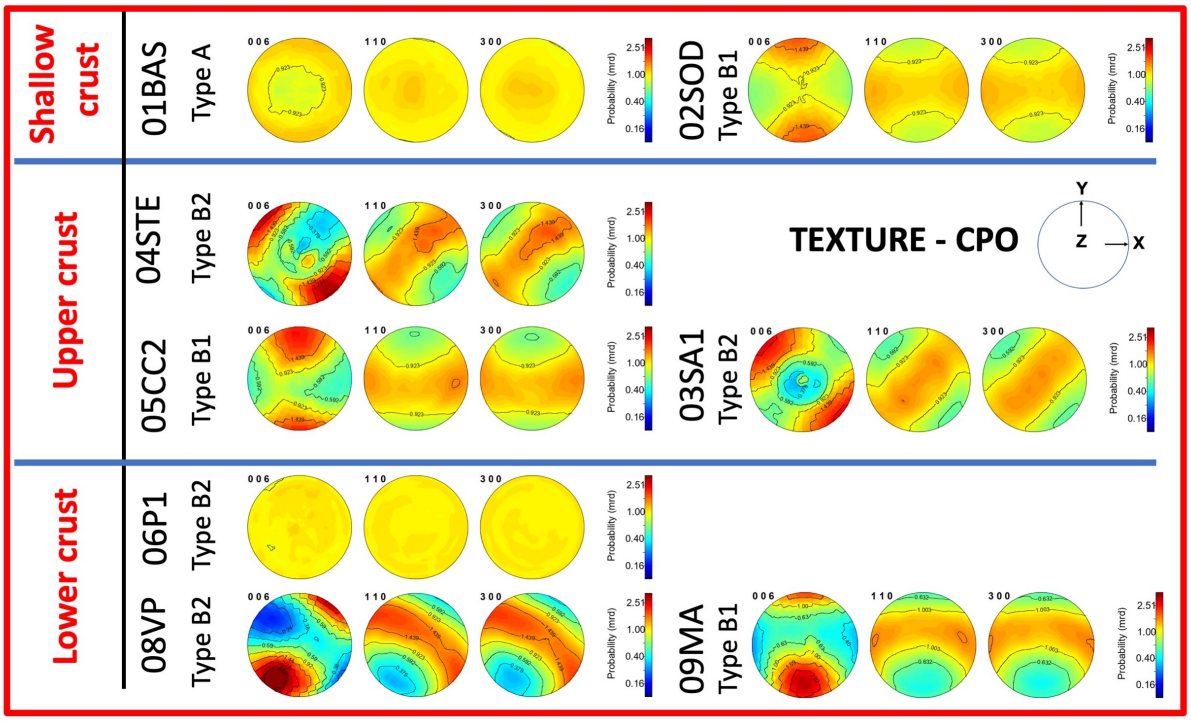

Figure 4. CPO Pole Figures for the studied sample. Axes reference as in Figure 2b

4.2. Seismic Velocities

Figure 5 reports the calculated seismic velocities. Namely, Vp (km/s), S-wave anisotropy and Vs1 polarization. Their distributions closely resemble the main CPO textural feature; in fact, since the c-axis direction is the slowest Vp in the single crystal setting, and the m-axes directions are the fastest (Figure 3), the general feature that shows up is that the pole to (006) distribution correspond to the slowest directions in the Vp plots. So, the prediction of the slowest direction in carbonatic rocks is straightforward since it is influenced by the c-axis distribution; in contrast, S-wave anisotropies are more complex to predict since they result from a combination of textural anisotropies (Figure 3). Specifically, 02SOD, 06P1, 08VP and 09MA display a girdle distribution, which correspond to a pronounced direction of fastest propagation. Conversely, 01BAS, 03SA1 and 05CC2 are characterized by single or multiple clusters for S-wave anisotropies, giving a more complex pattern of polarization. 07STE displays a mixed distribution, where the two clusters are linked by a weak fastest S-wave girdle.

Preprints (www.preprints.org) | NOT PEER-REVIEWED | Posted: 6 November 2019 doi:10.20944/preprints201911.0048.v1

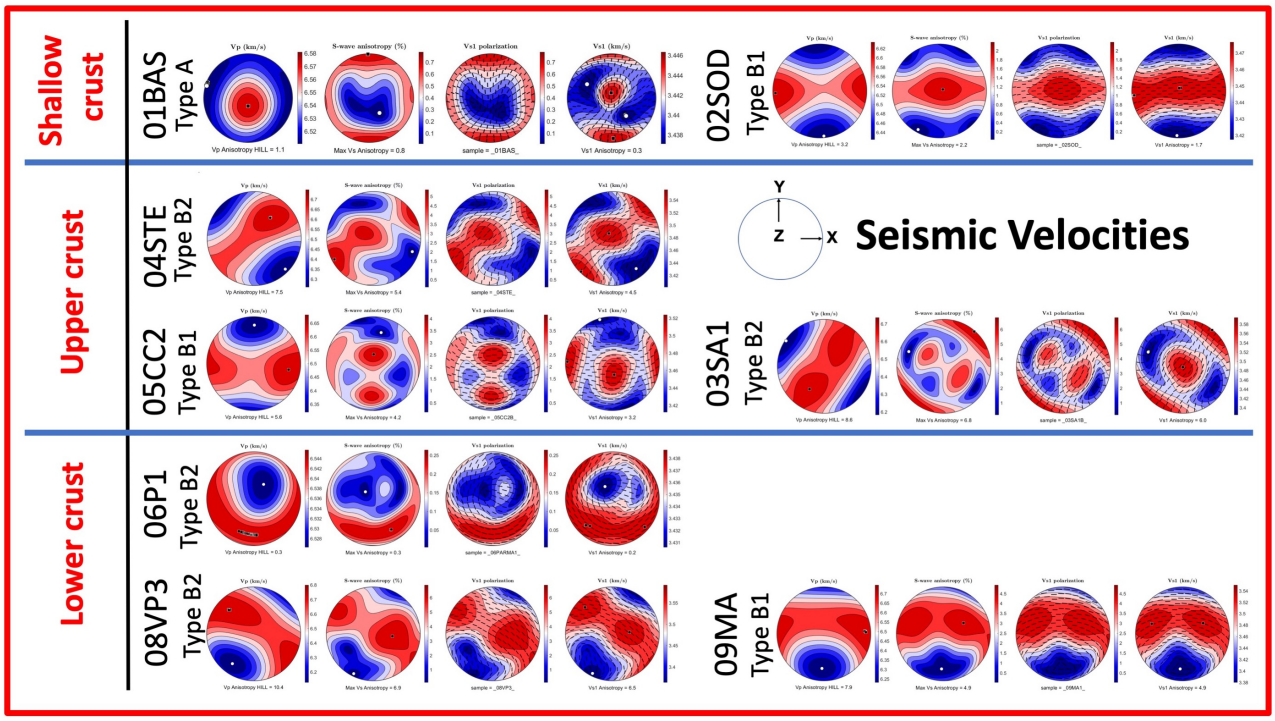

Figure 5. Vp(km/s), Vs velocities for the studied samples. Axes reference as in Figure 2b

Table 4. Homogenized Elastic Tensors for the studied samples - [GPa] - density = 2.712 g/cm3

Single Crystal

124.80639	54.72449	51.150898	0	-3.4680943	0
-	124.80639	51.150898	0	3.4680943	0
-	-	100.81746	0	0	0
-	-	-	30.698822	0	3.4680943
-	-	-	-	30.698822	0
-	-	-	-	-	35.04095

Model Bingham

127.50047	51.043633	55.929905	0	0	0
-	96.653496	51.04301	0	0	0
-	-	127.4964	0	0	0
-	-	-	30.140978	0	0
-	-	-	-	35.78422	0
-	-	-	-	-	30.141603

01BAS

115.48373	51.741405	52.193005	0.0137869865	-0.15203768	-0.057538427
-	115.00182	52.065735	-0.015753072	-0.070318885	-0.06224491
-	-	117.33802	0.003552162	-0.22920334	0.008067851
-	-	-	32.058846	0.005816382	-0.07812717
-	-	-	-	32.197884	0.013756884
-	-	-	-	-	31.695593

02SOD

 doi:10.20944/preprints201911.0048.v1

119.29561	51.75047	52.70474	0.09108701	-0.13749328	0.24086875
-	112.01606	51.493103	0.1646471	-0.030619144	0.2721084
-	-	116.93503	0.13448612	-0.15284155	0.118958846
-	-	-	31.385612	0.13175486	-0.03567471
-	-	-	-	32.75555	0.09919309
-	-	-	-	-	31.68194

03SA1

108.98519	51.129845	53.54879	-0.22707361	0.09098859	4.010708
-	115.68208	54.011932	-0.42028734	0.19944625	4.040168
-	-	120.24887	-0.4792106	0.6209795	1.0868437
-	-	-	34.00615	1.3028204	0.21294828
-	-	-	-	33.391453	-0.24855585
-	-	-	-	-	30.711746

04STE

114.62599	51.28098	52.65128	0.40403882	-0.24915834	4.076245
-	113.24674	52.87957	1.7690595	0.1510593	2.9629822
-	-	120.20226	1.3745261	-0.33024174	1.3390523
-	-	-	32.772617	1.5227332	0.12351844
-	-	-	-	32.543037	0.45559624
-	-	-	-	-	31.0105

05CC2

120.331055	52.018433	53.357944	-0.5572579	0.46192774	-0.14939365
-	109.84183	51.32877	-2.052971	0.22327025	-0.38076687
-	-	117.142975	-0.3637613	0.20798893	0.034985803
-	-	-	31.15168	0.02339253	0.23576291
-	-	-	-	33.43074	-0.6357612
-	-	-	-	-	31.877514

06P1

116.18255	52.0272	51.979866	-0.04868714	-0.03236508	-0.011777747
-	116.03572	51.9618	-0.16846395	-0.021853263	-0.021358635
-	51.9618	115.6278	-0.067962535	-0.08895395	-0.020873472
-	-	-	31.94424	-0.021930851	-0.02458574
-	-	-	-	31.965382	-0.053988267
-	-	-	-	-	32.021183

07P2

117.62099	51.808167	52.04327	0.26321256	0.320841	0.538134
-	115.71749	51.596924	0.7797489	0.24568443	0.40074456
-	-	115.65552	0.5507176	0.31947044	0.02256278
-	-	-	31.551678	0.03927036	0.26017663
-	-	-	-	32.037464	0.29400057
-	-	-	-	-	31.800737

08VP3

117.58365	52.024033	53.17902	0.9461038	1.649634	-5.2456484
-	111.576004	52.19252	3.4886246	0.64441526	-4.231288

Preprints (www.preprints.org) | NOT PEER-REVIEWED | Posted: 6 November 2019 doi:10.20944/preprints201911.0048.v1

-	-	119.872314	3.4239075	1.0557145	-1.510464
-	-	-	31.833376	-1.7366006	0.750887
-	-	-	-	32.96562	1.1209756
-	-	-	-	-	31.585485

09MA1

123.13773	51.935154	53.12128	1.066385	0.72052747	-0.34793347
-	108.63644	51.16951	3.118211	0.10843302	-0.30422294
-	-	117.85145	3.0853832	0.26028427	0.001484112
-	-	-	30.831026	-0.014819718	0.1207543
-	-	-	-	33.11233	1.2279662
-	-	-	-	-	31.690102

5. Discussion

The CPO data reported in Figure 4 represent the two **types of calcite texture** most commonly described for natural rocks [46] and reported in experimental results [13,14,47,48]. Namely, Type B textures (Fig. 4) reproduce the relations between the CPO and the shear plane described for pure shear (i.e. orthorhombic, Type B1) and simple shear (i.e. monoclinic, Type B2) deformation regimes [17,46]; those CPO asymmetries has been largely used to infer the deformation regime and the sense of shear [49–51]. However, [52] clearly demonstrated the risk simplifying those textural relations with deformational regimes. In fact, the most common calcite deformation mechanisms allow, even at low temperature, a quick transition from monoclinic to orthorhombic symmetries, even under a simple shear regime and at low strain (>2). Accordingly, the studied samples also show that discriminate between HT and LT textures, as suggested by [46] is not an easy task. For example, 02SOD, 05CC2 and 09MA samples though their textures developed at LT, IT and HT respectively (Table 1), they all display a similar orthorhombic symmetry; specularly, 04STE, 03SA1, 08VP even sharing the same texture, they developed at LT, IT and HT respectively (Figure 3, Table 1).

Thermodynamically modeled seismic velocities, Vp and Vs (Figure 6), describe a progressive increase of the Vp waves from $\approx$ 6.0 km/s at shallow depth to 6.5 km/s at the bottom of the lower crust. Otherwise, Vs velocities are almost constant ,from shallow to depth, from 2.9 to 3.1 km/s. These values largely differ from those calculated from the ODF obtained by means of the texture analysis (Figures 5, 7 and 8), as already noticed before [27]; this is true also for the modelled seismic velocities (e.g. single crystal, Uniform and Bingham distributions), as reported in figures 3 and 8.

Preprints (www.preprints.org) | NOT PEER-REVIEWED | Posted: 6 November 2019 doi:10.20944/preprints201911.0048.v1

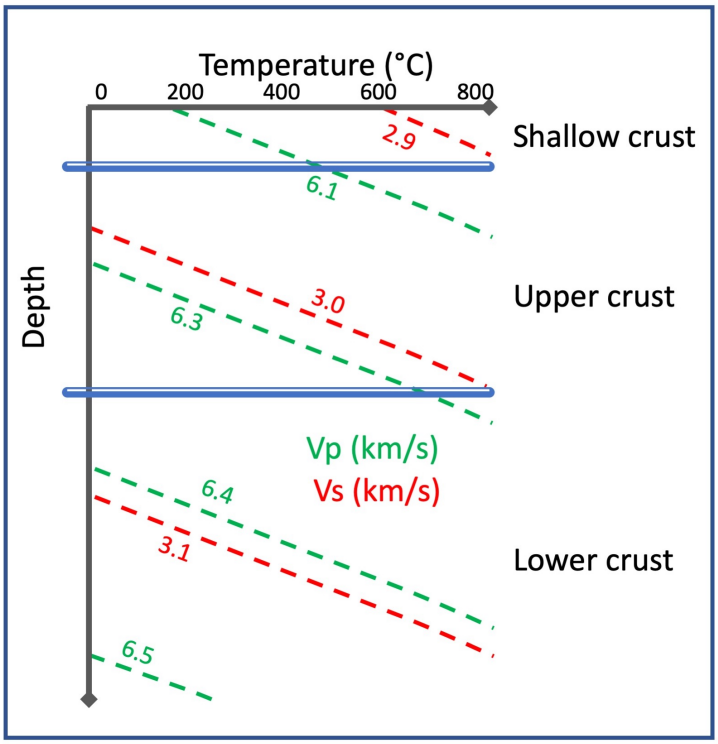

gv

Figure 6. P- and S-waves crustal profile, calculated using Perple_X thermodynamic packages [41].

Seismic velocities and anisotropy of calcite, in the studied samples, change with texture types (Figure 5). Vp velocities vary from a minimum of 6.2 km/s to a maximum of 6.8 km/s with the AVp anisotropy from 0 to 9.0 (Figure 5). Moreover, while the direction on maximum Vp, in the plane orthogonal to the XY mesoscopic fabric (e.g. shear and stratification), is generally parallel to X in orthorhombic fabrics, it lies at an angle that varies from 30 to 45 degrees. Furthermore, in the latter case, Vp max vector does not lie on the XZ plane but dip, gently to steep. S-wave anisotropy is also highly influenced by texture types and symmetries, leading to Max Vs Anisotropy varying from 0 to 7, and the Vs1 polarization (Figure 5). To better describe the variations of P- and S- wave with the dip angle of the shear plane, the homogenized elastic tensors (Table 4). Following the approach of Ko and Jung (2014) [53], the influence of dipping mesoscopic fabric on the seismic anisotropies is investigated by also changing the plane of view, from XZ, used since here for Pole Figure (Figures 3, 4, 5), to XY, by rotating 90 by X, and then, progressively, dipping the shear plane from 0 to 90 degrees, by rotate the Y axis. The 0, 30, 45, 70 and 90 steps are shown in Figure 7. From the resulting rotated tensors, the components of Vp, Vs1 and Vs2 are read parallel to the horizontal component of the X direction, as well the Vp component parallel to the orthogonal to the surface. Figure 7 and 8 show these results. In details, in Figure 7 the Pole Figures are such that the observer is looking down the Earth's surface (i.e. the Pole Figure plane), toward the Earth's core, and the planes of shear is plot at different dip angles. The center of the Pole Figure is the normal to the topographic surface, the Y axis is fixed while the fabric X and Z axes rotate. Moreover, the type of texture is reported, where Type A correspond to randomly distributed CPO, Type B preferred oriented CPO, separated in Type B1, orthorhombic distribution, and Type B2, monoclinic distribution.

Preprints (www.preprints.org) | NOT PEER-REVIEWED | Posted: 6 November 2019 doi:10.20944/preprints201911.0048.v1

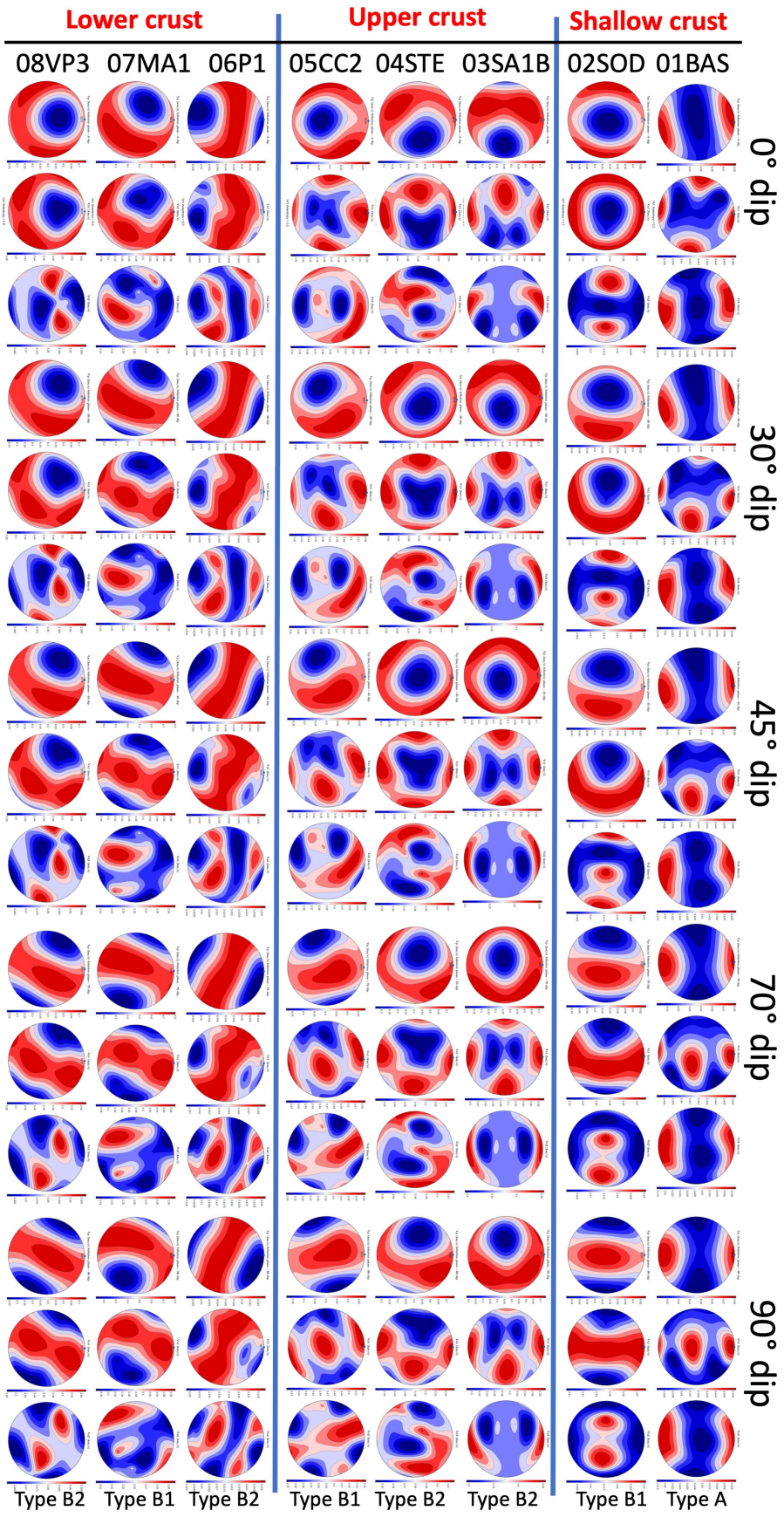

Figure 7. Pole Figures representing the P- and S- (S1 and S2) seismic velocities for calcite at different depth and dipping angle of the main macroscopic fabric plane (e.g. shear plane or stratification)

Preprints (www.preprints.org) | NOT PEER-REVIEWED | Posted: 6 November 2019 doi:10.20944/preprints201911.0048.v1

Figure 8 represents schematically the same variations, but taken normal to the topographic surface and within the topographic surface but orthogonal to the Y axis. These two directions correspond to the horizontal and vertical components of the X and Z axes. These data are represented in Figure 8 by the three texture types. In particular, Vp velocities in Type A random distribution remain constant varying the dip and the average Vp along the horizontal and vertical directions is at about 6.55 km/s, for both shallow and lower crust rocks. Those values deviate from both those of single crystal, above 6.75 km/s, and thermodynamic average, 6.0 km/s at shallow crust level and 6.2 at lower crustal levels (Figure 6). Similar features are shown for Vs1 and Vs2 components for the same Type A samples when compared with single crystal and thermodynamic average (Figure 8). More diverse feature arise with Type B distributions. In fact, orthorhombic Type B1 shows similar features for samples at different depth, with a general trend where Vp along horizontal decreases at steep dipping shear zones while the vertical component increases. The Vs1 component generally decreases for the three samples at different depth, but it is more steep for the lower crust sample (e.g. 08MA1). On the other hand, Vs2 components show that the upper crust sample 05CC2 has a different trend to the other samples.

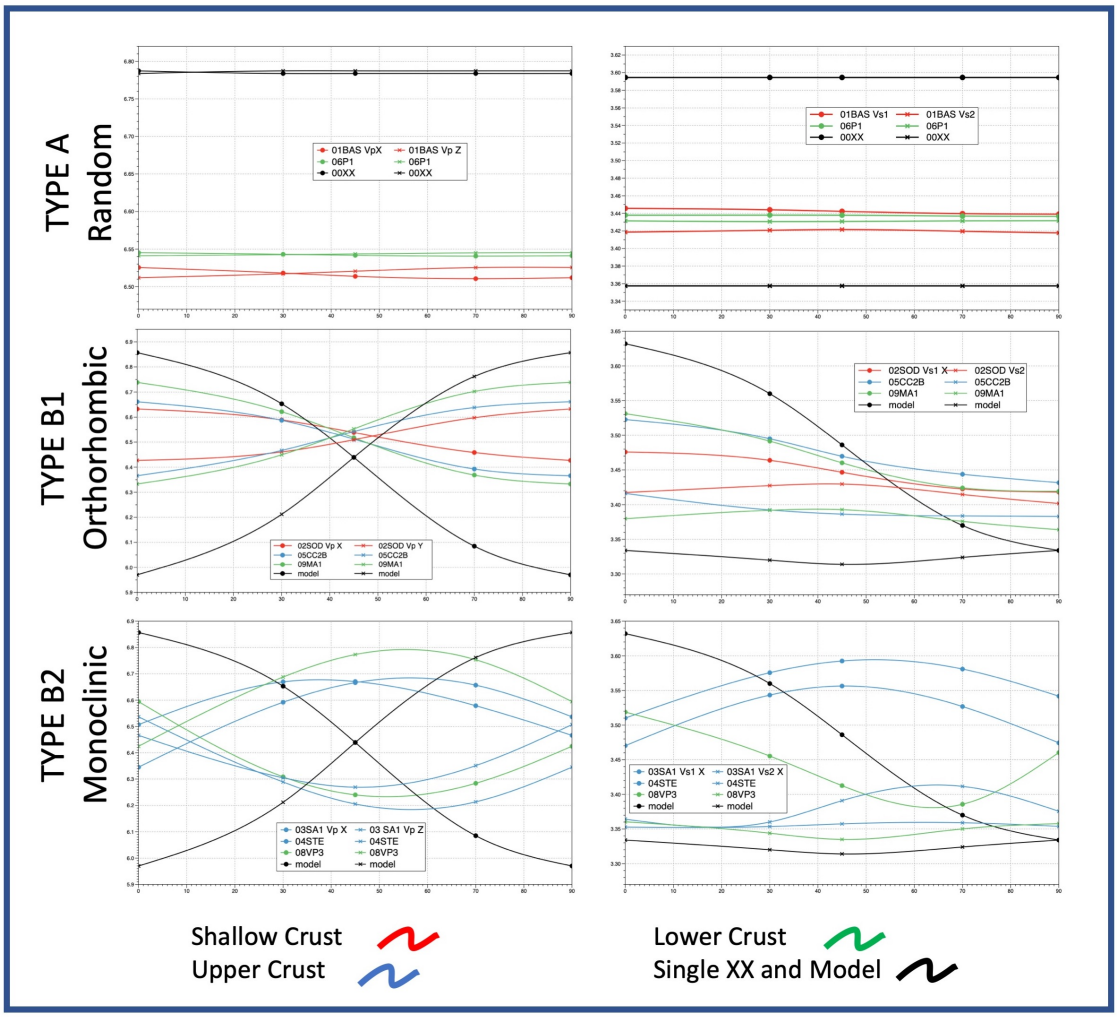

Figure 8. Vp components along horizontal X and Z - Vs1 and Vs2 along horizontal component of X

Preprints (www.preprints.org) | NOT PEER-REVIEWED | Posted: 6 November 2019 doi:10.20944/preprints201911.0048.v1

In the Type B2 monoclinic samples distribution, the lower crust sample 09VP3 display an opposite trend to the upper crust samples 03SA1 and 04STE. In particular, while for the upper crust samples the horizontal Vp and Vs1 values increase from 0 to 45-50 degrees and then decrease approaching vertical dipping, the lower crustal sample 08VP3 starts decreasing and then, at about 60 degrees dip, increases. These heterogeneities also occur for vertical Vp and Vs2 components. The Vp vertical component closely mirrors the Vp horizontal, while the Vs2 components are less sensitive to the dip variation, being in a smaller interval, generally < 0.1 km/s.

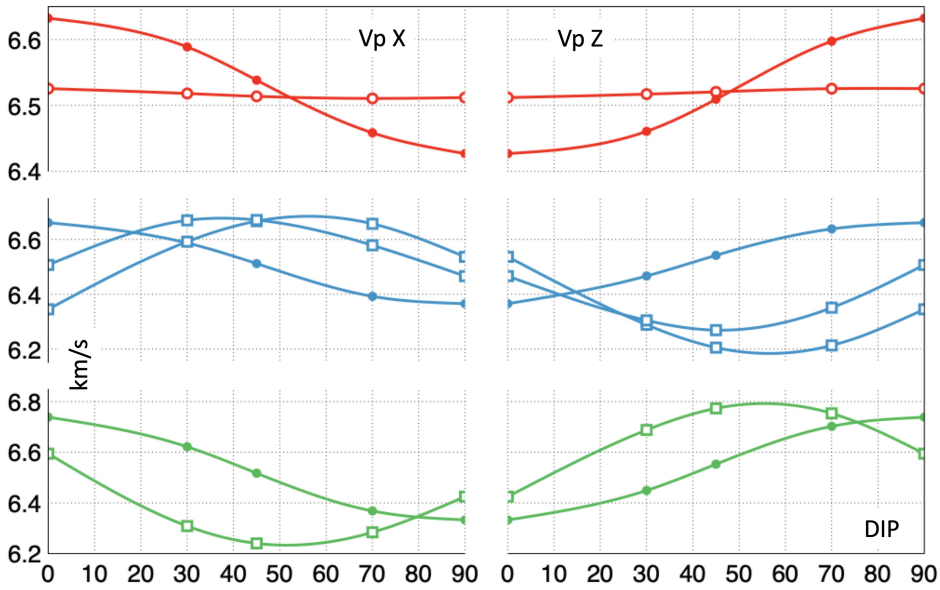

Figure 9. Vp crustal section. Shallow crust = red, Upper crust = blue, Lower crust = green. Texture types: A = hollow circle; B1 = full circle; B2 = hollow square

Figure 8 represents the Vp velocities at different depth, from shallow to lower crust. From 0 to 15 degrees dipping of the shear planes, as those normally developed along flat part of thrust systems [8], the Type B1 textures produce higher Vp velocities along the horizontal X component and slower parallel to the normal to the topographic surface. This setting does not change with depth, while the fastest VpX velocities are recorded at depth (i.e. lower crust). This pattern remains is reversed at different at different dip angles: shallow crust at 50 degrees, upper crust between 20 and 30 degrees, and the lower crust at 80 degrees. This flip may correspond, at upper crust conditions, to the evolution of the thrust system from flats to ramps, which may correspond to a strong increase of the Vp velocities along the horizontal X component, from 6.4 to 6.7 km/s, and the corresponding decrease through the direction orthogonal to the topographic surface, for rocks having a Type B2 CPO pattern. Oppositely, at depth, both Type B1 and B2 produce an overall decrease of the horizontal velocities, from 6.8 to 6.3 km/s and from 6.6 to 6.2 km/s, respectively. Even though, Type B2 reach their minimum at 50 degrees and then increase slowly moving toward vertical dips. In general, steep dipping shear zones, as those in trans-tensional or trans-pressional systems (e.g positive and negative flower structures), will produce slower or at maximum equal VpX velocities than shear zone within the same system but with lower dipping angles (Figure 9).

6. Conclusions

- Eight samples of limestones and marbles were studied by neutron diffraction. We collected CPO of naturally deformed calcite at different depths in the crust, from shallow to lower crust shear zones.
- Different CPO patterns were recognized, from random (Type A) to strongly textured (Type B); the latter, with orthorhombic (Type B1) or monoclinic (Type B2) symmetries. Seismic anisotropies were calculated using the Orientation Distribution Function to homogenize the elastic tensor of calcite.
- A wide variability of seismic anisotropies arise from the various textural types, crustal positions and dipping of the shear planes.
- These results may be valuably used to guess geometry of shear zones at shallow to depth for carbonatic rocks or at deeper crustal levels where thick carbonatic horizons are involved localizing deformation.
- The presented results and the approach used may become a reference for calculating reflection coefficients when interpreting seismic profiles.
- More work still needs to be done to include other parameters influencing seismic anisotropies, intrinsic and extrinsic, to build a database of natural rocks properties [5,55] , across the crustal profile from shallow to lower crust [6,39,54].

Author Contributions: All authors participated in the preparation of this manuscript. M.Z. conducted sample collection, collaborated neutron experiments, data analysis and prepared the first version of the manuscript. D.C. worked on neutron experimentsand data analysis. B.O. worked on neutron experiments and data analysis.

Funding: Neutron experiments were funded by ILL (www.ill.eu)

Acknowledgments:

Conflicts of Interest: The authors declare no conflict of interest.

References

1. Lowrie, W. *Fundamentals of Geophysics, second edition*; 2007; [arXiv:1011.1669v3]. doi:10.1017/CBO9780511807107.
2. Sun, L.; Fang, C.; Sa, L.; Yang, P.; Sun, Z. Innovation and prospect of geophysical technology in the exploration of deep oil and gas. *Shiyou Kantan Yu Kaifa/Petroleum Exploration and Development* **2015**, *42*, 414–424. doi:10.1016/S1876-3804(15)30038-0.
3. Kendair, J.M.; Maddock, J.; Hall, S.A.; Fisher, Q.J. Seismic anisotropy as an indicator of reservoir quality in siliciclastic rocks. *69th European Association of Geoscientists and Engineers Conference and Exhibition 2007: Securing The Future. Incorporating SPE EUROPEC 2007* **2007**, *5*, 2614–2618. doi:10.1144/SP292.7.
4. Okaya, D.; Vel, S.S.; Song, W.J.; Johnson, S.E. Modification of crustal seismic anisotropy by geological structures ("structural geometric anisotropy"). *Geosphere* **2019**, *15*, 146–170. doi:10.1130/GES01655.1.
5. Brownlee, S.J.; Schulte-Pelkum, V.; Raju, A.; Mahan, K.; Condit, C.; Orlandini, O.F. Characteristics of deep crustal seismic anisotropy from a compilation of rock elasticity tensors and their expression in receiver functions. *Tectonics* **2017**, *36*, 1835–1857. doi:10.1002/2017TC004625.
6. Almqvist, B.S.; Mainprice, D. Seismic properties and anisotropy of the continental crust: Predictions based on mineral texture and rock microstructure. *Reviews of Geophysics* **2017**, *55*, 367–433. doi:10.1002/2016RG000552.
7. Prior, D.J.; Mariani, E.; Wheeler, J. EBSD in the Earth Sciences : Applications , Common Practice , and Challenges EBSD in the Earth Sciences : Applications , Common Practice , and Challenges **2010**. doi:10.1007/978-0-387-88136-2.
8. Suppe, J. Geometry and Kinematics of fault-bend folding. *American Journal of Science* **1983**, *283*, 681–721.
9. Busch, J.P.; van der Pluijm, B.a. Calcite textures, microstructures and rheological properties of marble mylonites in the Bancroft shear zone, Ontario, Canada. *Journal of Structural Geology* **1995**, *17*, 677–688.

10. Bestmann, M.; Kunze, K.; Matthews, A. Evolution of a calcite marble shear zone complex on Thassos Island, Greece: Microstructural and textural fabrics and their kinematic significance. *Journal of Structural Geology* **2000**, *22*, 1789–1807. doi:10.1016/S0191-8141(00)00112-7.
11. Barber, D.J.; Wenk, H.R.; Gomez-Barreiro, J.; Rybacki, E.; Dresen, G. Basal slip and texture development in calcite: New results from torsion experiments. *Physics and Chemistry of Minerals* **2007**, *34*, 73–84. doi:10.1007/s00269-006-0129-3.
12. Pieri, M.; Kunze, K.; Burlini, L.; Stretton, I.; Olgaard, D.L.; Burg, J.P.; Wenk, H.R. Texture development of calcite by deformation and dynamic recrystallization at 1000 K during torsion experiments of marble to large strains. *Tectonophysics* **2001**, *330*, 119–140.
13. Schuster, R.; Habler, G.; Schafler, E.; Abart, R. Microstructural and textural evolution of calcite deformed to high shear strain by high-pressure torsion. *Journal of Structural Geology* **2019**, *118*, 32–47. doi:10.1016/j.jsg.2018.09.003.
14. Schmid, S.M.; Panozzo, R.; Bauer, S. Simple shear experiments on calcite rocks: rheology and microfabrics. *J. Struct. Geol. JOurnal of Structural Geology* **1987**, *9*, 747–778.
15. Maria, A.; Migliazza, M.; Spagnoli, A.; Zucali, M. Micromechanics of intergranular cracking due to anisotropic thermal expansion in calcite marbles. *ENGINEERING FRACTURE MECHANICS* **2014**, pp. 1–11. doi:10.1016/j.engfracmech.2014.01.004.
16. Lutterotti, L.; Matthies, S.; Wenk, H.R.; Schultz, a.S.J.; Richardson, J.J.W. Combined texture and structure analysis of deformed limestone from time-of-flight neutron diffraction spectra. *Journal of Applied Physics* **1997**, *81*, 594–600.
17. Leiss, B.; Molli, G. 'High-temperature' texture in naturally deformed Carrara marble from the Alpi Apuane, Italy. *Journal of Structural Geology* **2002**, *25*, 649–658.
18. BRGM - Carte géologique image de la France au million. http://geoservices.brgm.fr/geologie? Accessed: 2019-09-30.
19. ISPRA - Carta geologica d'Italia alla scala 1:500.000. Geoportale Cartografico Italiano. http://wms.pcn.minambiente.it/ogc?map=/ms_ogc/WMS_v1.3/Vettoriali/Carta_geologica.map&. Accessed: 2010-09-30.
20. Camana, G.; Chateigner, D.; Zucali, M.; Artioli, G. The grid-work texture of authigenic microcrystalline quartz in siliceous crust-type (SCT) mineralized horizons. *American Mineralogist* **2002**, *87*.
21. Wenk, H.R. Neutron diffraction texture analysis. In *In: Neutron Scattering in Earth Sciences, Reviews in Mineralogy and Geochemistry, 63*; Mineralogical Society of America, 2006; pp. 399–426.
22. Zucali, M.; Tartarotti, P.; Capelli, S.; Ouladdiaf, B. Multiscalar structural study of the ultramafic rocks of the Antrona ophiolite (Pennine Alps). In: (Eds.) Guido Gosso, Maria Iole Spalla, and Michele Zucali, Multiscale structural analysis devoted to the reconstruction of tectonic trajectories in active ma. *Journal of The Virtual Explorer* **2012**, *41*, 4.
23. Zucali, M.; Chateigner, D.; Dugnani, M.; Lutterotti, L.; Ouladdiaf, B. Quantitative texture analysis of glaucophanite deformed under eclogite facies conditions (Sesia-Lanzo Zone, Western Alps); comparison between X-ray and neutron diffraction analysis. *Geological Society Special Publications* **2002**, *200*, 239–253.
24. Siegesmund, S.; Helming, K.; Kruse, R. Complete texture analysis of a deformed amphibolite: comparison between neutron, diffraction and U-stage data. *Journal of Structural Geology* **1994**, *16*, 131–142.
25. Zucali, M.; Barberini, V.; Voltolini, M.; Ouladdiaf, B.; Chateigner, D.; Mancini, L.; Lutterotti, L. *Quantitative 3D microstructural analysis of naturally deformed amphibolite from the Southern Alps (Italy): Microstructures, CPO and seismic anisotropy from a fossil extensional margin*; Vol. 409, 2015. doi:10.1144/SP409.5.
26. Frassi, C.; Musumeci, G.; Zucali, M.; Mazzarini, F.; Rebay, G.; Langone, A. The Cotoncello Shear Zone (Elba Island, Italy): The deep root of a fossil oceanic detachment fault in the Ligurian ophiolites. *Lithos* **2017**, *278-281*. doi:10.1016/j.lithos.2017.02.015.
27. Zucali, M.; Voltolini, M.; Ouladdiaf, B.; Mancini, L.; Chateigner, D. The 3D quantitative lattice and shape preferred orientation of a mylonitised metagranite from Monte Rosa (Western Alps): Combining neutron diffraction texture analysis and synchrotron X-ray microtomography. *Journal of Structural Geology* **2014**, *63*. doi:10.1016/j.jsg.2014.02.011.

28. Zucali, M.; Fontana, E.; Panseri, M.; Tartarotti, P.; Capelli, S.; Ouladdiaf, B. Submarine lava flow direction revealed by neutron diffraction analysis in mineral lattice orientation. *Geochemistry, Geophysics, Geosystems* **2014**, *15*. doi:10.1002/2013GC005044.
29. Frischbutter, A.; Neov, D.; Scheffzük, C.; Vrána, M.; Walther, K. Lattice strain measurements on sandstones under load using neutron diffraction. *Journal of Structural Geology* **2000**, *22*, 1587–1600. doi:10.1016/S0191-8141(00)00110-3.
30. Tartarotti, P.; Zucali, M.; Panseri, M.; Lissandrelli, S.; Capelli, S.; Ouladdiaf, B. Mantle origin of the Antrona serpentinites (Antrona ophiolite, Pennine Alps) as inferred from microstructural, microchemical, and neutron diffraction quantitative texture analysis. *Ofioliti* **2011**, *36*, 167–189.
31. Lutterotti, L.; Matthies, S.; Wenk, H.R. MAUD (Material Analysis Using Diffraction): a user friendly Java program for Rietveld Texture Analysis and more. Proceedings of the Twelfth International Conference on Textures of Materials (ICOTOM-12),; Szpunar J. A.., Ed., 1999, Vol. 2, p. 1599.
32. Matthies, S.; Wenk, H.R.; Vinel, G.W. Some basic concepts of texture analysis and comparison of three methods to calculate orientation distributions from pole figures. *Journal of Applied Crystallography* **1988**, *21*, 285–304. doi:10.1107/S0021889888000275.
33. Babuska, V.; Cara, M. *Seismic anisotropy in the Earth*; Vol. 10, Springer, 1991.
34. Mainprice, D.; Hielscher, R.; Schaeben, H. Calculating anisotropic physical properties from texture data using the MTEX open-source package. *Geological Society, London, Special Publications* **2011**, *360*, 175–192. doi:10.1144/SP360.10.
35. Mainprice, D.; Humbert, M.; Wagner, F. Phase Transformations and Inherited ODFs Implications for Petrophysical Properties. *Textures and Microstructures* **1991**, *14*, 339–345. doi:10.1155/TSM.14-18.339.
36. Hill, R. The Elastic Behaviour of a Crystalline Aggregate. *Proceedings of the Physical Society. Section A* **1952**, *65*, 349–354. doi:10.1088/0370-1298/65/5/307.
37. Burlini, L.; Kunze, K. Fabric and seismic properties of Carrara marble mylonite. *Physics and Chemistry of the Earth, Part A: Solid Earth and Geodesy* **2000**, *25*, 133–139. doi:10.1016/S1464-1895(00)00022-3.
38. Burlini, L.; Marquer, D.; Challandes, N.; Mazzola, S.; Zangarini, N. Seismic properties of highly strained marbles from the Splügenpass, central Alps. *Journal of Structural Geology* **1998**, *20*, 277–292. doi:10.1016/S0191-8141(97)00084-9.
39. Faccenda, M.; Ferreira, A.M.; Tisato, N.; Lithgow-Bertelloni, C.; Stixrude, L.; Pennacchioni, G. Extrinsic Elastic Anisotropy in a Compositionally Heterogeneous Earth's Mantle. *Journal of Geophysical Research: Solid Earth* **2019**, *124*, 1671–1687. doi:10.1029/2018JB016482.
40. Faccenda, M.; Bressan, G.; Burlini, L. Seismic properties of the upper crust in the central Friuli area (northeastern Italy) based on petrophysical data. *Tectonophysics* **2007**, *445*, 210–226. doi:10.1016/j.tecto.2007.08.004.
41. Connolly, J.A. Multivariable phase diagrams: an algorithm based on generalized thermodynamics, 1990. doi:10.2475/ajs.290.6.666.
42. pyWerami (v 0.25) - a stand-alone program to make an countour/3D plot from data file generated by the PerpleX program WERAMI or tci file generated by TCInvestigator. https://github.com/ondrolexa/pywerami, 2017.
43. Fisher, N.I.; Lewis, T.; Embleton, B.J.J.B.J.J. *Statistical analysis of spherical data*; Cambridge University Press, 1993; p. 329.
44. Chateigner, D. Reliability criteria in quantitative texture analysis with experimental and simulated orientation distributions. *Journal of Applied Crystallography* **2005**, *38*, 603–611. doi:10.1107/S0021889805013695.
45. Schaeben, H. Texture analysis of heterogeneous data–a farewell to F-coefficients. *Journal of Structural Geology* **2000**, *22*, 1565–1568.
46. Wenk R, H.; Takeshita, T.; Bechler, E.; Erskine G, B.; Matthies, S. Pure shear and simple shear calcite textures; comparison of experimental, theoretical and natural data. *Cobbold, Cobbold*, **1987**, *Peter*, Denis,.
47. Burlini, L.C.M.; Rutter, E.H.; Anonymous. Preferred orientation development in hot-pressed synthetic, ultrafine-grained calcite rocks. *Terra Abstracts* **1993**, *5, Suppl.*, 288.

48. Casey, M.; Rutter, E.H.; Schmid, S.M.; Siddans, A.W.B.; Whalley, J.S. Texture development in experimentally deformed calcite rocks. *proc. 5th ICOTOM, Göttstein & Lücke (eds) proc. 5th ICOTOM, Göttstein & Lücke (eds)* **1978**, *2*, 231–240.
49. Schmid, S.M.; Casey, M.; Starkey, J. The microsfabric of calcite tectonites from the Helvetic Nappes (Swiss Alps). *in: Thrust and Nappe Tectonic, Geol. Soc. London in: Thrust and Nappe Tectonic, Geological Society of London* **1981**, pp. 151–158.
50. Ratschbacher, L.; Wenk, H.R.; Sintubin, M. Calcite textures; examples from nappes with strain-path partitioning. *Journal of Structural Geology* **1991**, *13*, 369–384.
51. Erskine G, B.; Heidelbach, F.; Wenk R, H. Lattice preferred orientations and microstructures of deformed Cordilleran marbles; correlation of shear indicators and determination of strain path. *Kirby, Kirby,* **1993**, *Stephen*, A.
52. Pieri, M.; Burlini, L.; Kunze, K.; Stretton, I.; Olgaard, D.L. Rheological and microstructural evolution of Carrara marble with high shear strain: Results from high temperature torsion experiments. *Journal of Structural Geology* **2001**, *23*, 1393–1413.
53. Ko, B.; Jung, H. Crystal preferred orientation of an amphibole experimentally deformed by simple shear. *Nature Communications* **2015**, *6*, 1–10. doi:10.1038/ncomms7586.
54. Almqvist, B.S.; Hirt, A.M.; Herwegh, M.; Ebert, A.; Walter, J.M.; Leiss, B.; Burlini, L. Seismic anisotropy in the Morcles nappe shear zone: Implications for seismic imaging of crustal scale shear zones. *Tectonophysics* **2013**, *603*, 162–178. doi:10.1016/j.tecto.2013.05.025.
55. Lloyd, G.E.; Butler, R.W.H.; Casey, M.; Tatham, D.J.; Mainprice, D. Constraints on the seismic properties of the middle and lower continental crust. *From: Prior, D. J., Rutter, E. H. & Tatham, D. J. (eds) Deformation Mechanisms, Rheology and Tectonics: Microstructures, Mechanics and Anisotropy. Geological Society, London Special Publications.* **2011**, *360*, 7–32.